The Influence of Multi-cellular Natural Convection Heat Transfer in the Oxide Pool of the Three-Layer Configuration

Ji-Won Bae and Bum-Jin Chung*
Department of Nuclear Engineering, Kyung Hee University
#1732 Deogyoung-daero, Giheung-gu, Yongin-si, Gyeonggi-do, 17104, Korea
**Corresponding author:bjchung@khu.ac.kr*

1. Introduction

In a severe accident, the corium relocates to the lower reactor vessel and radiates the decay heat continuously. The cooling of the corium using IVR-ERVC (In-Vessel Retention-External Reactor Vessel Cooling) is good measure to maintain the reactor vessel integrity and prevent the release of radioactive materials into the containment [1].

When the molten fuels retain in reactor vessel, it is stratified into two-layer or three-layer. In the three-layer configuration, the upper metal layer becomes thinner, which intensifies the heat focusing from upper metal layer to the reactor vessel. Therefore, especially in the three-layer configuration, it is more important to investigate the influence of height of layers. However, the existing studies on the three-layer configuration are rare as the interest in the possibility of three-layer formation has only grown recently [2-3].

The experimental study was performed to confirm the effect of aspect ratio (H/R) of the oxide layer under the equivalent decay heat condition. We measured local heat transfer coefficients (h_h) at the top plate, the curved side wall and the bottom plate for three different aspect ratios. The range of Ra'_H was from 6.70×10^{10} to 5.13×10^{13}. The Sc, which corresponds to Pr was 2,014. Based upon the analogy between heat and mass transfer, mass transfer experiments were performed in a copper sulfate–sulfuric acid ($CuSO_4$-H_2SO_4) electroplating system.

2. Theoretical background

2.1. Phenomena for oxide pool

The melted core is stratified into two types according to accident scenarios: Two-layer configuration, Three-layer configuration. In case of the two-layer, the light metal layer consists of Fe and Zr and oxide layer consists of UO_2 and ZrO_2 (Fig. 1(a)). If there is a large amount of non-oxidized Zr, U in the oxide layer migrates to the light metal layer and forms the heavy alloys. Then, the density of the upper metal layer is greater than oxide layer, which makes layer inversion as shown in Fig. 1(b). This phenomenon was confirmed by the MASCA experiments [4]. The upper metallic layer has no internal heat source but transfers the heat received from the oxide layer to the reactor vessel. It is called Focusing effect, which is more critical in three-layer configuration as the light metal and oxide layer becomes thinner than two-layer. In addition, for the same thickness of light metal layer, the depth of oxide layer is important because the heat load from the middle to the upper layer will alter with the depth of the oxide layer. The upper light metal layer contains Fe and Zr for 3-layer configuration. The middle oxide layer includes UO_2, ZrO_2 and most existing fission products. The lower heavy metal layer consists of U, Zr, Fe and some metallic fission products.

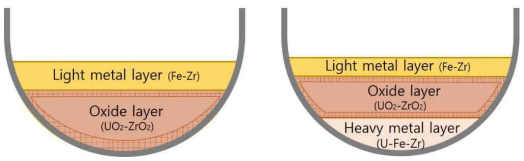

(a) Two-layer configuration (b) Three-layer configuration

Fig. 1. The composition of layer according to the configuration type [3].

As shown in Fig. 2, Kim and Chung [3] presented the flow patterns for three-layer configuration according to the aspect ratio. In Fig. 2(a), due to the external cooling, the natural convection flows run down along the curved surface, gathers at the bottom plate and move upward. At the top plate, gathered flows are dispersing from the center to the edge. These seem to symmetrical 'twin-cell' flow. Also, natural convective flows called secondary flows are formed underneath the top plate [5]. If the depth of oxide layers is shallow, the number of cells would be increase, creating 'multi-cell' flow as shown in Fig. 2(b).

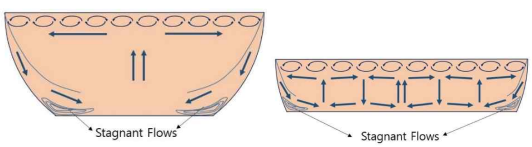

(a) Twin-cell (b) Multi-cell

Fig. 2. Flow pattern for three-layer configuration according to the aspect ratio [3].

2.2. Definition of Ra'_H

The oxide layer releases the decay heat continuously. Thus, the modified Rayleigh number

(Ra'_H) is defined as the multiplication of the conventional Rayleigh number (Ra_H) and Damköhler number (Da_H). The Da_H is a dimensionless parameter including the volumetric heat generation (q'''). The Ra'_H is expressed by

$$\boldsymbol{Ra'_H = Ra_H \times Da_H = \frac{g\beta\Delta T H^3}{\alpha\nu} \times \frac{q''' H^2}{k\Delta T} = \frac{g\beta q''' H^5}{\alpha\nu k}}, \quad (1)$$

$$\text{where } \boldsymbol{Da_H = \frac{q''' H^2}{k\Delta T}}. \quad (2)$$

2.3. Previous studies

Segal *et al.* [6] conducted the heat transfer experiments and simulated three-layer configuration with a 2-D semi-circular facility using paraffin oil (upper layer), water (middle layer) and chlorobenzene (lower layer). The heights of them are 5 cm, 18 cm, 4 cm respectively. The heater is located on 4 cm - 20 cm and supplies heat to entire middle layer and part of upper layer. The Ra'_H ranged from 6.01×10^{12} to 7.82×10^{12}. Their heat flux distribution at the vessel increased with the angle and peaked at the middle of the oxide layer. This does not account for the focusing effect at the upper metal layer.

Kim *et al.* [2] confirmed the natural convection in oxide layer of three-layer configuration and compared with two-layer configuration. This experimental study used 2-D semi-circular MassTER-OP2(HML) (Mass Transfer Experimental Rig for a 2-D Oxide Pool with Heavy Metal Layer) having flat bottom. The radius and width are 10 cm and 4 cm each. The height of 5.65 cm corresponds to aspect ratio of 0.56, which is determined by code calculation result in Park *et al.* [7]. The Ra'_H varied from 1.49×10^{12} to 1.36×10^{13}. They reported that the heat load on the top plate and top of the side wall was higher than that of the two-layer configuration, making the focusing effect more severe.

Kim and Chung [3] studied the effect of the aspect ratio (H/R) on the natural convection heat transfer in oxide layer through the experiments. The height of MassTER-OP2(HML) is 0.028 cm, 0.056 cm, 0.078 cm, which corresponds the Ra'_H from 7.51×10^{11} to 4.30×10^{13}. They expected that the multi-cell flow formed at 0.28 in aspect ratio (H/R) unlike the 0.56, 0.78 using the measured local heat transfer.

3. Experiments

3.1. Experimental methodology of mass transfer

Heat and mass transfer are analogous. This means that the two systems have the same mathematical expressions. Therefore, the heat transfer problems can be usually replaced by the mass transfer experiments [8].

The limiting current technique is a method of measurement used by the mass transfer system and several researchers developed this technique [9-12], and the methodology is so far well-established [13-15].

By using the mass transfer methods, we could accomplish most characteristics of molten oxide pool properly: high Ra'_H with small facilities, uniform heat generation and isothermal cooling condition.

3.2. Experimental apparatus

Figure 3 shows the MassTER-OP2(HML). They have same radial and width with previous MassTER-OP2: 0.1 m, 0.04 m, respectively. But heights are different as bottom of apparatus is chopped with various ratios, which are ranged to 0.028 m, 0.038 m and 0.047m. The heights are adopted between 0.028 m and 0.056 m to identify where the twin-cell begins to change into multi-cell in reference to Kim and Chung [3]. The Ra'_H is varied from 6.70×10^{10} to 5.13×10^{13}. The cathode copper plates are located on the inner wall of the top, curved side and bottom. The halves of cathode are single electrodes. And the other halve at the top, bottom and side wall are divided into 8, 4 and 8 electrodes, respectively, so as to measure the local current values and confirm the flow patterns in detail. The trapezium anode coppers that simulate internal heat sources are attached at the both side plates. The facilities are filled with copper sulfate–sulfuric acid ($CuSO_4$-H_2SO_4) solution.

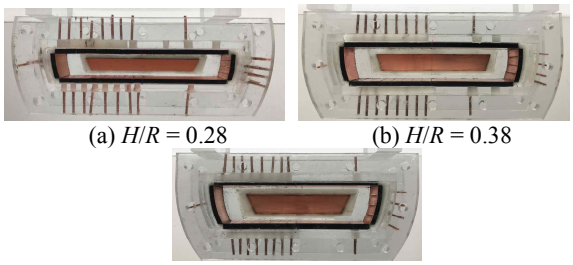

(a) H/R = 0.28 (b) H/R = 0.38

(c) H/R = 0.47

Fig. 3. Experimental apparatus.

In the IVR strategy, downward flows is caused along the side wall by external cooling so that the upward flows are formed at the certain points of the bottom toward the top plate. However, in the electroplating system, the cathode simulates a heated wall as cupric ions are reduced at the cathode causing the decrease of fluid density and resulting upward buoyancy. In order to position the cathode on the side wall, the direction of gravity must be reversed. Thus, the experiments were conducted at the inverted circuit as shown in Fig. 4. Some of studies tested with inverted circuit and their results agreed with existing correlations [14-15].

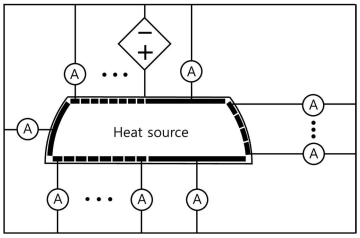

Fig. 4. Test circuit.

3.3. Test matrix

Table I presents the test matrix of this study. The experiments were performed for four different cooling condition of top and bottom plate. The side walls were maintained in isothermal condition in all cases. These conditions were predicted to the extreme cooling situation. The real conditions in severe accident will be included in between these extrema.

Table I: Test matrix.

Boundary condition			*Sc* (*Pr*)
Top	Side	Bottom	
Isothermal	Isothermal	Isothermal	*2,014*
		Insulated	
Insulated		Isothermal	
		Insulated	

4. Results and Discussions

Figure 5 shows the local heat transfer at the bottom plate for different aspect ratios (*H*/*R*). The x-axis and y-axis indicates the local position of bottom plate from center to edge and the normalized heat transfer coefficients (h^*) for equivalent decay heat condition, respectively. The overall tendency of results seems to increase from edge to center. This is similar with result of Kim and Chung [3] tested with large aspect ratio forming the twin-cell. In large aspect ratio, the flow moving toward the center is heated by the decay heat until rising at the center. The temperature difference between heating flow and bottom plate increases as the bottom plate has poor cooling ability compared to the received decay heat from the oxide layer. As the result, the heat transfer increases along the path of flow. The maximum value at position = 0.625 and minimum value at position = 0.425 are observed. When *H*/R is small, the driving force for natural convection is weak as the cooling side wall is short so that some of flows does not reach the center, resulting in some of rising flow at position = 0.625. Due to these rising flows at the position = 0, 0.625, the downward flow forms at position = 0.425. As the results, the multi-cell flow forms for the small *H*/*R* as shown in Fig. 2(b).

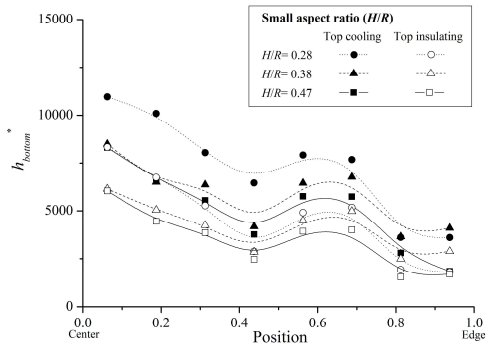

Fig. 5. Local heat transfer at the bottom plate for aspect ratios of 0.28, 0.38 and 0.47.

Figure 6 indicates the local heat transfer at the top plate for different *H*/*R*. Unlike the bottom plate, the effect of multi-cell on the top plate is minor as the secondary flows are formed underneath the top plate. On the other hand, overall results show a maximum value at position = 0.625. However, at too small *H*/*R* of 0.28, the peak is higher as the effect of the multi-cell flow on the top plate enhanced. The cooling condition of bottom plate does not influence the local result. Because the heat transfer at the top plate is higher than that of the bottom plate.

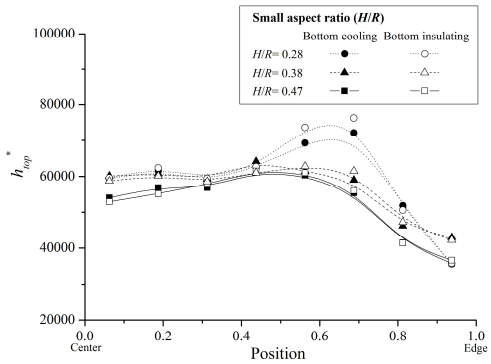

Fig. 6. Local heat transfer at the bottom plate for aspect ratios of 0.28, 0.38 and 0.47.

Figure 7 compares the ratios of upward heat to total decay heat (Q_{up}/Q_{tot}) for different aspect ratios (*H*/*R*). The upward heat ratio of *H*/*R* = 0.56, 0.78 is results of the Kim and Chung [3]. At large *H*/*R* forming the twin-cell flow, Q_{up}/Q_{tot} increases according to decrease of *H*/*R*. However, for the small *H*/*R* forming the multi-cell flow, the increase of Q_{up}/Q_{tot} is nearly constant although the *H*/*R* decreases. Because the multi-cell flow distributes the heat concentrated at the top evenly.

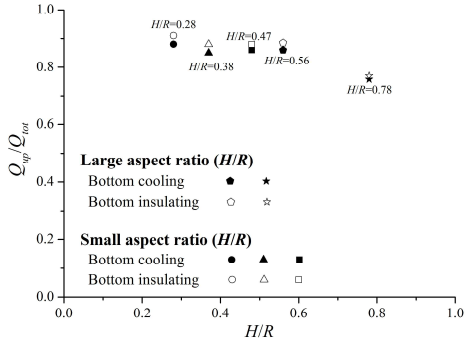

Fig. 7. Upward heat ratios according to the aspect ratio.

5. Conclusion

This study investigated the influence of aspect ratios in the oxide layer on the heat load from the oxide layer to the upper light metal layer. We performed the mass transfer experiments based on analogy concept between heat and mass transfer to achieve the high buoyancy using the small experimental apparatus.

Through the measurements of local heat transfer, we envisaged the flow patterns in detail at the small H/R. The local heat transfer at the bottom plate increased from the edge to the center with fluctuations due to the upward and downward flows at midway of the bottom plate. When the H/R is small, the driving force for the natural convection is weak as the cooling side wall is short. As the results, we observed multi-cell flow at the small H/R. The local heat transfer at the top plate did not reveal the effect of multi-cell directly as the heat transfer by the secondary flow formed the underneath of the top plate is much higher than the main flow. The cooling condition of the bottom plate has little influence on the heat transfer of the top plate as the heat transfer at the top plate is much higher than that of the bottom plate.

We confirmed that the heat load from the oxide layer to the upper light metal layer is varied depending on the flow patterns for the three-layer configuration. For large H/R forming the twin-cell, the upward heat ratios increased. However, for the small H/R forming the multi-cell, the increase of the upward heat ratios is nearly constant although the H/R decreases as the multi-cell flow distributes the heat concentrated at the upper light metal layer to the overall oxide layer.

ACKNOWLEDEGEMENT

This study was sponsored by the Ministry of Science and ICT (MSIT) and was supported by Nuclear Research & Development program grant funded by the National Research Foundation (NRF) (Grant code: 2017M2A8A4015283).

REFERENCES

[1] J. L. Rempe, K. Y. Shu, F. B. Cheung, S. B. Kim, In-vessel retention of molten corium: lessons learned and outstanding issues, Nuclear technology Vol. 161, pp. 210-267, 2008.
[2] Kim *et al.*, Natural convection of the oxide pool in a three-layer configuration of core melts, Nuclear engineering and design Vol. 317, pp. 100-109, 2017.
[3] Kim and Chung, Natural convection heat transfer of the oxide layer varying the aspect ratios for a three-layer configuration, Transactions of the Korean Nuclear Society Spring Meeting, 2017.
[4] Barrachin, M., Defoort, F., Thermophysical properties of In-Vessel Corium: MASCA Programme Related Results. Proceedings of MASCA Seminar, Aix-en-Provence, France, 2014.
[5] J. M. Bonnet and J.M. Seiler, "Thermal hydraulic phenomena in corium pools: The BALI experiment," 7th International Conference on Nuclear Engineering, Tokyo, Japan, 1999.
[6] B. R. Sehgal *et al.*, Natural convection heat transfer in a stratified melt pool with volumetric heat generation, 6th International topical meeting on nuclear reactor thermal hydraulics, operations and safety (NUTHOS-6), Nara, Japan, 2004.
[7] R. J. Park *et al.*, Corium behavior in the lower plenum of the reactor vessel under IVR-ERVC condition: technical issues, Nuclear Engineering and Technology Vol. 44, 2012.
[8] A. Bejan, Convection heat transfer. third ed, New York: John Wiley & Sons, INC, pp. 96-97, 173-179, 197-200, 512-516, 2006.
[9] V.G. Levich, Physicochemical Hydrodynamics, Prentice-Hall, Englewood Cliffs, New Jersey, 1962.
[10] J.N. Agar, Diffusion and convection at electrodes, Discuss. Faraday Soc. Vol. 26, pp. 27-37, 1947.
[11] C.W. Tobias, R.G. Hickman, Ionic mass transfer by combined free and forced convection, Int. J. Res. Phys. Chem. Chem. Phys Vol. 229, pp. 145-166, 1965.
[12] E.J. Fenech, C.W. Tobias, Mass transfer by free convection at horizontal electrodes, Electrochim. Acta 2, pp. 311-325, 1960.
[13] Bae *et al.*, Visualization of natural convection heat transfer inside an inclined circular pipe, International Communications in Heat and Mass Transfer, Vol. 92, pp. 15-22, 2018.
[14] Park *et al.*, Variation in the angular heat flux of the oxide pool with Rayleigh number, Annals of Nuclear Energy, Vol. 170, pp. 128-135, 2017.
[15]. Kim and Chung, Heat load imposed on reactor vessel during in-vessel retention of core melts, Nuclear Engineering and Design, Vol. 308, pp. 1-8, 2016